

Two Dimensional Numerical Simulation and Experimental Verification Flow Characteristics of an Involute Spur Gear Pump

Tsai-Shou Chang*, Jyun-Jie Wang** and Shinn-Liang Chang***

Keywords: Gear Pumps, Involute Gear, FEA, Efficiency Analysis.

Abstract

Gear pumps are popularly applied in industry, so, there are many researches published in the past years. However, there are few numerical simulations on the influence of contact point for outlet mass flow rate. In recent years, it is pointed out that the contact point must be considered in numerical simulation for cases whose outlet pressure is high, because the outlet flow rate of gear pump is significantly changed.

In this study, a two dimensional numerical and the associated experimental study were conducted to explore the effect of contact point on the characteristics of an involute spur gear pump. Besides, the relationships of the displacement efficiency, the rotation speed, and the pressure of outlet of a gear pumps are investigated. The range of the above mentioned parameters are numerically and experimentally investigated. The experiments showed good match with the analysis results proposed in this paper.

1. Introduction

The hydraulic transmission is a transmission form in which a liquid is used as the medium for energy transmission and control. The system is mainly composed of a power component, an actuator component, a control component, an auxiliary component, and a working medium. The hydraulic change of the sealed working space to achieve the suction and discharge of oil, thereby transforming the input mechanical energy into a device that outputs hydraulic energy. According to the structural characteristics of the hydraulic pump, it can be generally divided into a piston pump, a vane pump, and a gear pump.

Paper Received January, 2021. Revised June, 2021. Accepted July, 2021. Author for Correspondence: Shinn-Liang Chang

* Associate Professor, Department of Power Mechanical Engineering, National Formosa University, Taiwan 63201, ROC.

** Graduate Student, Department of Power Mechanical Engineering, National Formosa University, Taiwan 63201, ROC.

*** Professor, Department of Power Mechanical Engineering, National Formosa University, Taiwan 63201, ROC.

Gear pumps are rotary type pumps in the positive displacement pump. Taking the gears as the main structure, gears are used to squeeze the hydraulic oil into the system to drive the entire hydraulic system to work. The static pump, also known as the positive displacement pump, supplies a certain amount of liquid to the system at every revolution. Under ideal conditions, the output flow should be independent of the outlet pressure, but in actual operation, the pump flow is reduced by internal leakage, which is exacerbated by the increase of outlet pressure.

Zakharov and Ibragimov (1964) directed the working fluid in the high-pressure oil discharge area to the rear end of the pressure plate, and the pressure plate was brought closer to the gear set through the back pressure to narrow the gap to reduce leakage. Hooke and Koc (1984) performed pressure plate force analysis on compensating and pressure-compensated pressure plates to predict the gap between the pressure plate and the gear end face. It was found that the leakage between the gear surface and the pressure plate was the largest.

Koc and Hooke (1988) explained the relationship between the pressure plate and the side clearance of the gear and the amount of leakage. It shows that the gap size will affect the amount leakage. Koc et al. (1997) measured the clearance between the bushing side of the bushing gear pump and the side of the gear, and analyzed the lubrication mechanism. A brief description of the volumetric efficiency loss and slip source caused by slip was illustrated by Nelik (2001). Castilla et al. (2010) found that in the case of an outlet pressure higher than 10 bar, in the numerical simulation, the contact point is closed to obtain a more accurate outlet flow rate. Castilla et al. (2015) changed the viscosity of fluid at the contact point to achieve the closing effect. A pair of gears with 1.4 contact ratio is simulated by the laminar flow.

According to the foregoing literature review, only Castilla et al. (2010) had proposed research on contact point closure. However, this method has not been further studied on gear pump efficiency and other characteristics. This study uses numerical methods to further develop this method for accurate numerical simulation results.

1.1 Theoretical displacement

The theoretical displacement of the gear pump is:

$$\dot{V}_{net} = \dot{V}_o - \dot{V}_s \quad (1)$$

where \dot{V}_o is the output volume flow rate, and \dot{V}_s is the theoretical flow rate of the return volume flow rate. There are different calculation methods for each revolution of gear pump theory. For a gear pump consisting of gears with equal number of teeth, the volume of liquid discharged by one revolution of the main shaft is equal to the sum of the volumes of the two teeth. For standard gears, the gear tooth volume is equal to the tooth space volume, so the geometric displacement of the gear pump is equal to the sum of the tooth volume and the tooth space volume of a gear, as shown in Eq. (2).

$$Q = 2\pi m^2 z b \quad (2)$$

where m is module, z is numbers of teeth, and b is the thickness of the gear.

Consider the volume difference between the tooth body and tooth space, a correction coefficient f can be induced, as shown in Eq. (3).

$$Q = 2\pi f m^2 z b \quad (3)$$

where f is the modification coefficient, $1.05 < f < 1.15$.

2. Numerical simulation of flow field of an involute external spur gear pump

2.1 Model settings

The structure of the gear pump used in this research includes the front plate, bottom plate, gear plate, gear set, and bearings, etc. The perspective view and exploded view are shown in Figures 1 and 2, respectively.

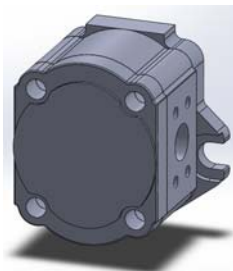


Figure 1 Perspective view of gear pump

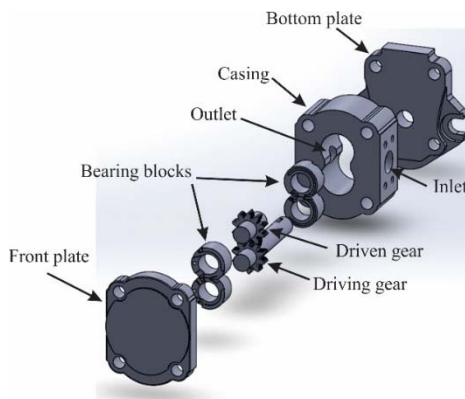


Figure 2 Exploded view of gear pump

2.2 Analysis of transient flow field of gear pump

Efficiency and life are the two most important indicators of the quality of gear pumps, among which the outlet flow of the gear pump is an important indicator of quality. In this section, the characteristics of the mass flow rate at the outlet of the gear pump are discussed by changing parameters such as center distance, speed, and outlet pressure.

In this study, a 2D gear pump volume model was used, with the gear as the rotor, the center of the driving gear as the origin of the coordinates. The positive value on the right is set as the X axis, and the positive value on the upper is set as Y axis, as shown in Figure 3.

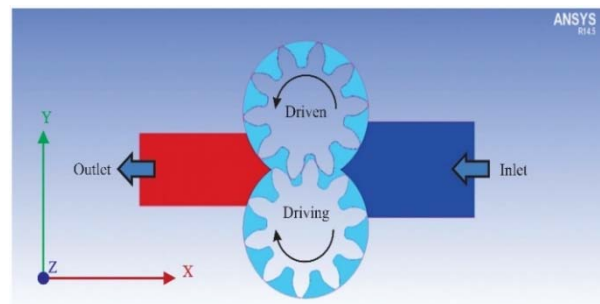


Figure 3 Gear pump flow field space

2.2.1 Governing equation

Under the assumption that the fluid is an incompressible viscous fluid and the physical properties of the fluid are constant, the basic governing equations can be derived. The continuity equation, momentum equation and turbulence equation are described as follows:

Continuity equation

$$\frac{\partial}{\partial x_i} (\rho u_i) = 0 \quad (4)$$

Momentum equation

$$\frac{\partial}{\partial t} (\rho u_i) + \frac{\partial}{\partial x_j} (\rho u_i u_j) = -\frac{\partial p}{\partial x_i} + \frac{\partial}{\partial x_i} \left[\mu \left(\frac{\partial u_i}{\partial x_j} + \frac{\partial u_j}{\partial x_i} - \frac{2}{3} \delta_{ij} \frac{\partial u_l}{\partial x_l} \right) \right] + \frac{\partial}{\partial x_j} (-\rho \overline{u'_i u'_j}) \quad (5)$$

where u_i and u_j are the velocity components of x and y , p is the static pressure, ρ is the density, μ is the viscosity coefficient, and $-\rho \overline{u'_i u'_j}$ is the Reynolds stress.

Turbulent mode

In ANSYS Fluent, the turbulence mode uses the $k-\epsilon$ module, which is divided into Standard $k-\epsilon$, RNG $k-\epsilon$, and Realizable $k-\epsilon$ mode. In terms of experiments, Ertürk et al. (2008) used Time Resolved Particle Image Velocimetry (TRPIV) measurement technology to observe the actual state of turbulence in the flow field. In the numerical simulation, Castilla et al. (2010) used the above three turbulence modes and laminar flow for analysis. The simulation and experimental results are compared with each other, and finally the turbulence

simulated by the RNG k-ε mode is more in line with reality. Because the gear pump is susceptible to turbulence at the inlet and outlet positions, the gear pump model uses the RNG k-ε model. The turbulent flow energy k equation and dissipation rate ε equation are composed as follows.

Turbulent flow energy k equation:

$$\frac{\partial}{\partial t}(\rho k) + \frac{\partial}{\partial x_i}(\rho k u_i) = \frac{\partial}{\partial x_j} \left[\alpha_k \mu_{eff} \frac{\partial k}{\partial x_j} \right] + G_k + G_b - \rho \varepsilon - Y_M \tag{6}$$

Dissipation rate ε equation:

$$\frac{\partial}{\partial t}(\rho \varepsilon) + \frac{\partial}{\partial x_i}(\rho \varepsilon u_i) = \frac{\partial}{\partial x_j} \left[\alpha_\varepsilon \mu_{eff} \frac{\partial \varepsilon}{\partial x_j} \right] + C_{1\varepsilon} \frac{\varepsilon}{k} (G_k + C_{3\varepsilon} G_b) - C_{2\varepsilon} \rho \frac{\varepsilon^2}{k} \tag{7}$$

Among them, G_k is the turbulent flow energy generated based on the average velocity gradient; G_b is the turbulent flow energy generated based on buoyancy; Y_M is the overall dissipation rate of fluctuation expansion in compressible turbulence; $\alpha_k = \alpha_\varepsilon \approx 1.393$.

Boundary settings are mainly divided into exit, entrance, and flow field spaces as shown in Figure 4. The preset pressure of inlet pressure is one atmosphere, that is, the gauge pressure is 0. The outlet gauge pressure is set to 0, 2, 4, 6, and 8 MPa, as shown in Figure 4.

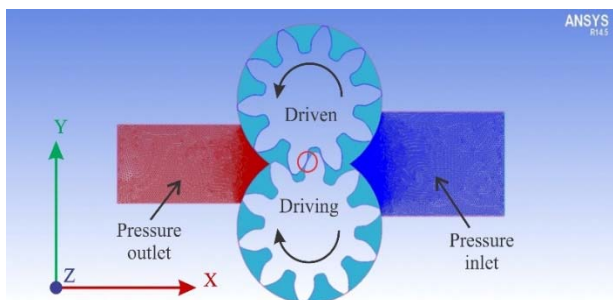


Figure 4 Boundary and grid type distribution of each region

2.2.2 Simulation related settings

(1) Dynamic mesh

The flow field space is mainly divided into three areas: the entrance, the exit, and the gear rotation area. The gear rotation area is subdivided into a driving gear area, a driven gear area, and a flow area, respectively. Enlarge the meshing area from the red circle in Figure 4, as shown in Figure 5. Because the geometry of the gear pump is very complicated, the grid construction method uses an unstructured grid, and the grid shape is a triangle grid.

When the boundary changes with time, the dynamic mesh model can simulate the change of the flow field. Gear pump is a rotating machinery, so when using Fluent, it is often necessary to use dynamic mesh models for simulation. The dynamic grid update process is automatically calculated based on the boundary

changes during each time step.

(2) The closed setting of engagement area

During the simulation process, the meshing process of the gear pump did not form a closed area as it actually is, for two reasons:

1. The driving gear and the driven gear are driven individually; the contact point cannot be obtained automatically.
2. The flow field space is divided by the grid. During the simulation, the grid at each point must return values at any time to calculate the flow field state. If the engineer wants to break the grid to form a true closed area, it will cause the grid to rupture and calculations are failed.

In order to solve this situation, the method proposed by Castilla et al. (2010) is applied to set a closed area on the contact point making the flow field closed. Firstly, the position of the contact point is derived from the geometry, and a program is written in C language. The viscosity at the contact point is set to be much higher than the viscosity of the original working fluid, to achieve a state that the contact point is closed.

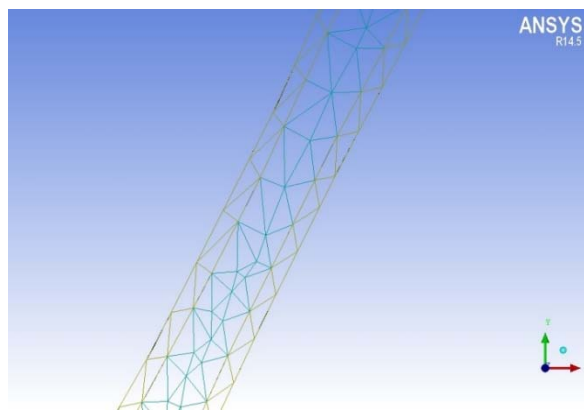


Figure 5 Division of gear flow area and distribution of grid pattern

2.2.3 Simulation results of transient flow field

Mass flow rate characteristics at different center distances

The center distances of the gear pump used in this simulation are 32.92 and 33.00 mm. The long-term average outlet mass flow rate of the two models at different gear speeds is compared. The fixed outlet gauge pressure is 0MPa.

The results are shown in the Table 1. The outlet mass flow rates of two different center distances are linearly distributed under a fixed outlet pressure, and increase with the increase of the speed. In addition, it can be observed that the exit mass flow rate of the model with a center distance of 32.92mm is slightly higher, and the difference is between 1% and 2%. Therefore, the results show that the numerical simulation results of the center distance variation having little effect on the export mass flow rate.

Table 1 Outlet mass flow rate under different center distances and rotating speed

Rotating speed	32.92mm Exit mass flow rate(A)	33.00mm Exit mass flow rate(B)	Export mass flow rate difference (B)/(A)
900	13.6035	13.4678	99.00%
1100	16.6034	16.4325	98.82%
1300	19.6456	19.4560	99.03%
1500	22.6530	22.4019	98.84%
1700	25.6179	25.3851	98.82%
1800	27.2006	26.9290	99.00%

Flow field characteristics at different speeds and outlet pressures

Here, the mass flow rate and displacement characteristics at different speeds and different outlet pressures are discussed.

(1) Instantaneous change of mass flow rate

Figure 6 shows the instantaneous mass flow rate change for a cycle of gear pump engagement when the speed is 1700 rpm and the back pressure is 4 MPa. The gear meshing starts at point 1 and ends at point 9 in the figure, and point 9 is also the starting point of the next meshing cycle.

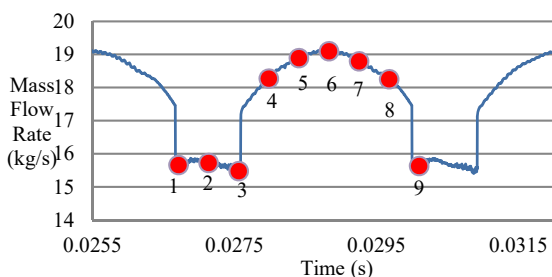


Figure 6 The position of instantaneous mass flow rate change

Figure 7(1)~(8) correspond to the flow field velocity distribution of points 1~9 in Figure 6. The relationship of the mass flow rate change can be observed more clearly from the outlet flow rate. Figure 7(1)~(3) means that the gear pump just starts to mesh. Because there are two meshing points, the maximum pressure is enclosed in the meshing area. At this time, the outlet flow rate is slightly oscillating; Figure 7(4)~(6) indicates a pair of gear teeth before the meshing area. The mesh has been disengaged, only a pair of gear teeth are left meshing, and the high pressure in the meshing area is gradually released toward the outlet area, so the outlet flow rate starts to climb at this time, and the flow rate is the fastest in Figure 7(6). At this time, the meshing point has passed through the center of the gear and gradually moved away from the exit area, causing its flow velocity to begin to decrease, as shown in Figure 7(7)~(8). Finally, return to Figure 7(1) and repeat the next cycle.

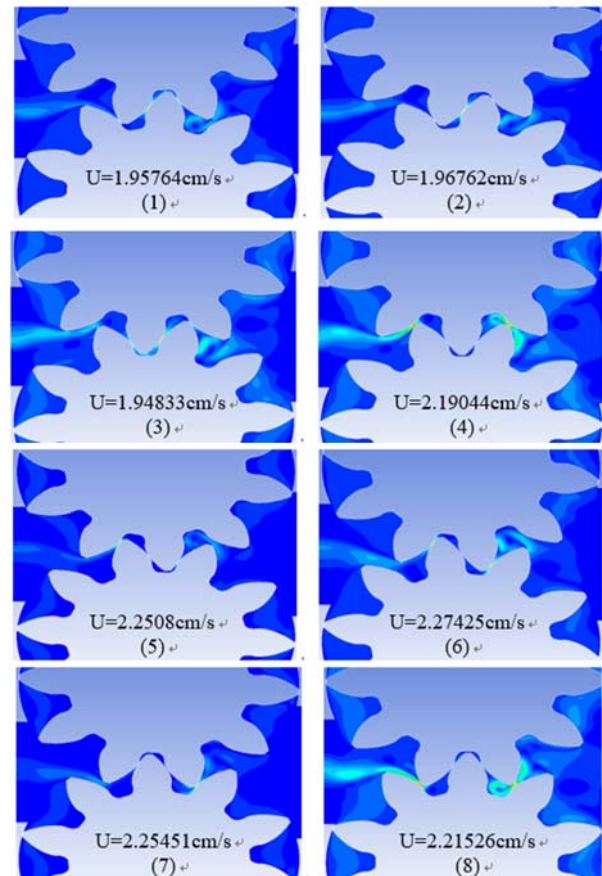


Figure 7 Instantaneous flow field velocity distribution with a time of 0.0267099s~0.0296779s

(2) Fixed outlet pressure at 0 MPa and 8 MPa

Figure 8 shows the average mass flow rate of the outlet gauge pressure 0 and 8 MPa.

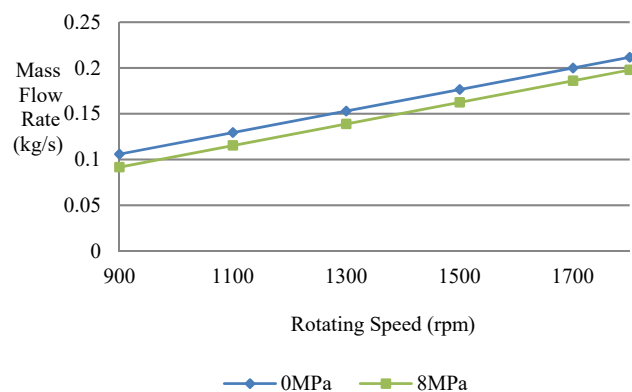


Figure 8 Long-term average mass flow rate at outlet gauge pressure 0 MPa and 8 MPa

As the speed is increased, the average mass flow rate will also increase linearly. This is because the gear pump tooth space volume is fixed, as the speed increases, the flow rate increases. Figure 9 shows the displacement of outlet gauge pressure 0 and 8 MPa. As the rotation speed is increased, the displacement of each speed at the outlet gauge pressure 0 MPa is constant, and the displacement

of the outlet gauge pressure 8 MPa increases as the speed increases. This is because the gear pump's tooth volume is fixed, and its output is not affected by the speed when the outlet pressure is no-load. When the outlet pressure increases, the leakage increases, making the no-load displacement higher than the outlet pressure of 8 MPa. In addition, under the condition of fixed outlet pressure, the lower speed causes the poor self-priming ability of the gear pump, and a more leakage. It makes the higher speed with a higher displacement.

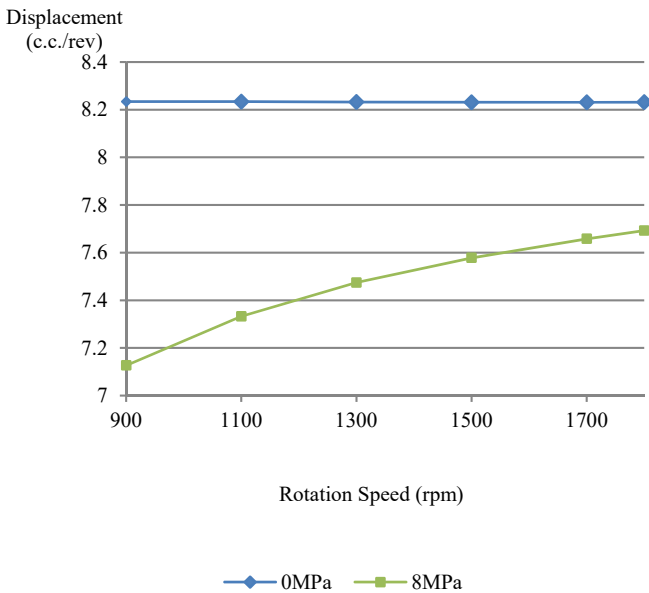


Figure 9 Displacement of outlet gauge pressure 0 MPa and 8 MPa

(3) Fixed speeds of 900 and 1800 rpm

Figure 10 shows the changes of the average mass flow rate and outlet pressure at fixed speeds 900 and 1800 rpm, respectively. Higher outlet pressures will cause the lower outlet mass flow rates.

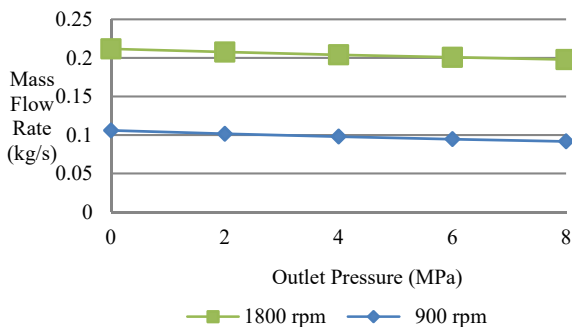


Figure 10 Characteristics of long-term average mass flow rate and pressure at 900 and 1800 rpm

Figure 11 shows the characteristics of displacement and outlet pressure at fixed speeds 900 and 1800 rpm, respectively. Due to the increase in outlet pressure, the internal pressure difference of the gear pump becomes larger, which in turn causes the leakage amount to increase. Therefore, the larger outlet pressure

causes the lower displacement, and a higher speed causes a higher displacement because the gear pump tooth space volume is fixed.

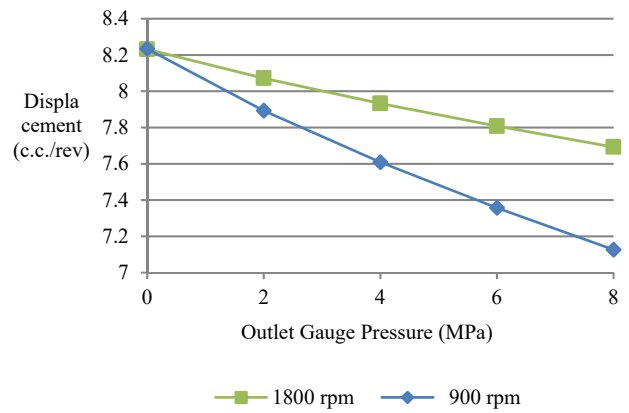


Figure 11 Displacement and outlet gauge pressure characteristics at speeds of 900 and 1800 rpm

(4) Mass flow rate spectrum analysis

Figure 12 shows the distribution of the mass flow rate at the outlet of a gear pump with pressure 0 MPa and 900 rpm. It can be seen from the figure that the mass flow rate shows a periodic change.

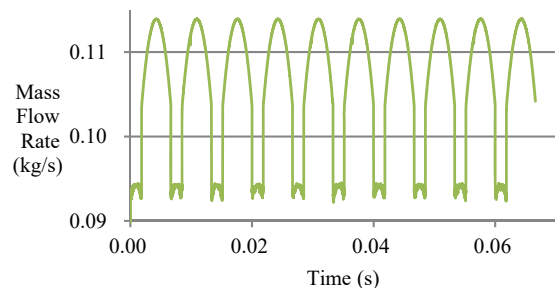


Figure 12 Periodic changes in mass flow rate

Set an observation point at the gear pump outlet ($x = -18.61\text{mm}$, $y = 16.46\text{mm}$), and observe the speed in the X and Y directions at this point. The Figure 13 shows the trajectory phase diagram of the outlet gauge pressure 0 MPa and 900 rpm. The vertical axis is the speed v in the Y direction and the horizontal axis is the speed $u - \bar{u}$ in the X direction, where u is the speed in the X direction and \bar{u} is the average speed in the X direction. Applying the Fourier transfer to analyze the frequency spectrum, it was found that the peaks appeared at frequencies of 149 Hz, 299 Hz, and 449 Hz, which are multiples of 150 Hz. Therefore, 150 Hz is the main frequency of the flow field, and the other frequencies are frequency doublings as shown in Figure 14.

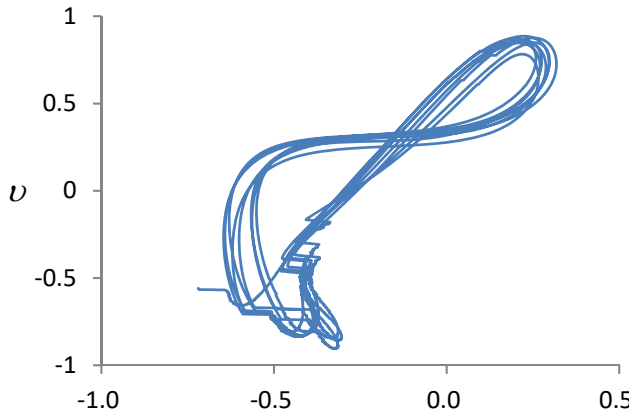


Figure 13 Phase diagram of velocity locus of observation points (-18.61mm, 16.46mm), outlet gauge pressure 0 MPa, speed 900 rpm

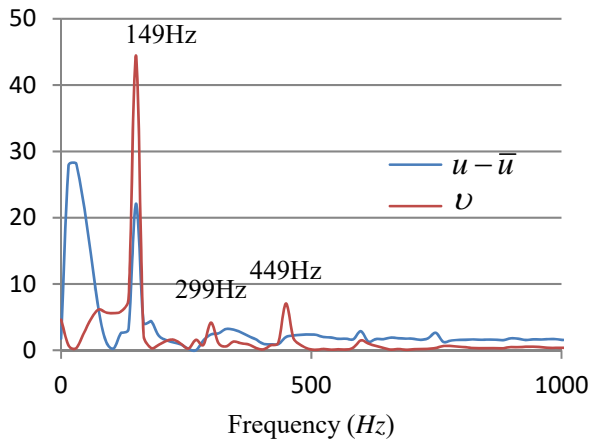


Figure 14 Spectral graph of observation point (-18.61mm, 16.46mm), Outlet gauge pressure 0 MPa, speed 900 rpm

When the outlet pressure is fixed and the speed is increased to 1800 rpm, the distribution in the trajectory phase diagram is more dispersed, as shown in the Figure 15.

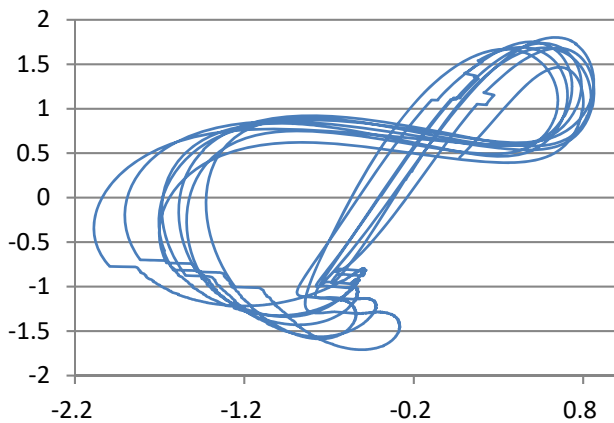


Figure 15 Speed trajectory phase diagram of observation point (-18.61mm, 16.46mm), outlet gauge pressure 0 MPa, speed 1800 rpm

The peaks of $u - \bar{u}$ spectrum are at frequencies 302 Hz, 604 Hz, and 907 Hz, respectively. The frequencies appear based on multiples of 300 Hz. It can be determined here that the frequency at 300 Hz is the main frequency of $u - \bar{u}$, and the other frequencies are multipliers. The frequency peaks of the speed v are at the frequencies 302 Hz, 604 Hz, 876 Hz, 967 Hz, 1209 Hz, and 1511 Hz. The frequencies appear based on multiples of 300 Hz, of which 876 Hz and 967 Hz are not multiples of 300 Hz. Here are the factors that cause the 1800 rpm trajectory phase map to be scattered compared to 900 rpm, as shown in the Figure 16.

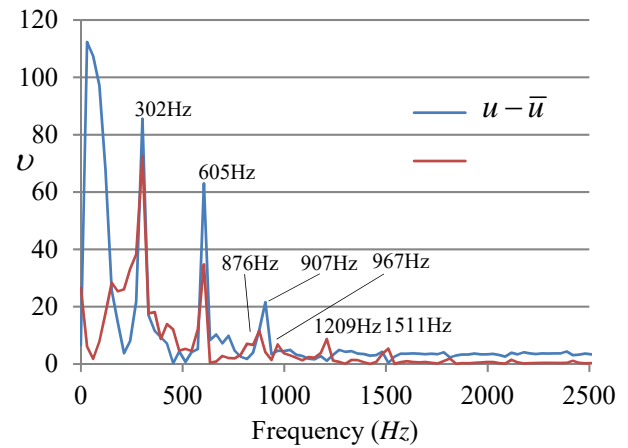


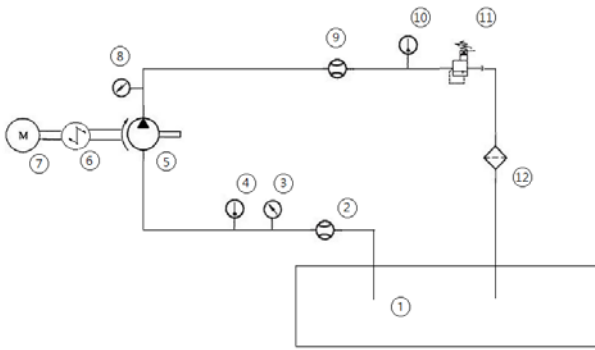
Figure 16 Spectral diagram of observation point (-18.61mm, 16.46mm), outlet gauge pressure 0 MPa, speed 1800 rpm

3. Comparison between the experiment and analysis

3.1 Experimental test machine

In this research, through experiments and simulations, and mutual verification of theory, the experimental machine is mainly composed of the console, hydraulic system and sensor. The detailed configuration is shown in the Figure 17.

When the power is turned on and the motor starts to run, the gear pump is driven and the values of speed and torque are transmitted back to the system. The pilot-operated relief valve at the outlet end acts to cause a pressure difference between the outlet and the inlet. According to this action, the gear pump starts to suck the working fluid from the inlet into the low-pressure area, and then the fluid is discharged to the high-pressure area at the outlet. Currently, it flows through the sensor area and the sensor returns data such as pressure, flow and temperature to the system. Finally, the working fluid passes the cooler to reduce the working temperature and flows back to the oil barrel. Figure 17 shows the system diagram of the experimental machine, and the Figure 18 shows the gear pump test machine in this study.



1-Water tank, 2-Vane flow sensor, 3-Pressure sensor, 4-Thermometer, 5-Quantitative gear pump, 6-Torque sensor, 7-Motor, 8-Pressure sensor, 9-Vane flow sensor, 10- Thermometer, 11-Pilot operated relief valve, 12-Cooler.
Figure 17 Test machine system diagram



Figure 18 Gear pump test machine

3.2 Experimental methods and uncertainty analysis

(1) Experimental methods

Adjust the rotation speed to 900, 1100, 1300, 1500, 1700, and 1800 rpm respectively, then adjust the relief valve so that the outlet gauge pressure is no load, 2.0, 4.0, 6.0, and 8.0 MPa. According to the designed different outlet pressure, from low to high, under the condition of fixed outlet pressure, the gear pump outlet flow, and input torque and speed are measured at different speeds in order to calculate efficiency.

(2) Uncertainty analysis

For the calculation of experimental inaccuracy, Kline and Mcclintock (1953) provided an accurate method of calculation. This method is based on a detailed classification of experimental measurement equipment. Set the measurement equipment in the experimental machine to the independent variables $x_1, x_2, x_3, \dots, x_n$ in the R function, as shown in the Eq. (8).

$$R = R(x_1, x_2, x_3, \dots, x_n) \quad (8)$$

Substituting the variables in Eq. (8) into Eq. (9), the total W_R of the system uncertainty can be shown as:

$$W_R = \left[\left(\frac{\partial R}{\partial x_1} w_1 \right)^2 + \left(\frac{\partial R}{\partial x_2} w_2 \right)^2 + \dots + \left(\frac{\partial R}{\partial x_n} w_n \right)^2 \right]^{\frac{1}{2}} \quad (9)$$

where w_i is an independent variable of uncertainty.

Use Eq. (9) to calculate the uncertainty of hydraulic power, mechanical power, volumetric efficiency, mechanical efficiency and total efficiency. The independent variables are flow, pressure and torque. The results are shown in Table 2.

Table 2 Uncertainty of each item

Items	uncertainty
Hydraulic power	1.376%
Mechanical power	2.105%
Volume efficiency	0.154%
Mechanical efficiency	3.482%
Total efficiency	3.617%

3.3 Comparison of theoretical, simulation, and experimental results

In this section, the theoretical values, simulations, and experimental results are compared. The theoretical values are calculated from Eq. (2). Among the three methods, only the experimental method considers the side clearance leakage.

Table 3 shows the comparison of the numerical simulation, experiment, theoretical formula, and the volume of the tooth space when the outlet pressure is at no load and the speed is 900 ~ 1800 rpm. It shows that the theoretical displacement obtained by Eq. (3) and simulation, are higher than the experimental value having the side clearance leakage.

Table 3 Displacement comparison of gear pump at no-load

Items	Displacement (c.c.)
Numerical Simulation	8.23
Experiment	8.05
Eq. (2)	8.14
Volume of Gear Pump Tooth Space	8.27

When the outlet gauge pressure is no-load, the output displacement of the gear pump does not change with the speed. Conversely, when the outlet gauge pressure is 8 MPa, the output displacement starts to increase with the increase of the speed, as shown in the Figure 19. Consider the fluid flow, no matter whether the outlet gauge pressure is no load or 8 MPa, the flowrate will increase with the increase of the speed, as shown in the Figures 20 and 21. In addition, because the displacement uncertainty is very small, the error interval is not marked on the chart.

The above results show that the simulated mass flow rate and displacement results are higher than the experimental results. The main reason is that the experimental gear pump is three-dimensional having

side leakage. There are three types of gap in the gear pump, i.e., the gap between the top surface of the gear and the pump casing, the gap between the side of the gear and the pressure plate, and the gap in the gear contact area. The leakage between the side of the gear and the pressure plate is the highest. Therefore, in the two-dimensional simulation, the leakage is greatly reduced, which leads to higher outlet mass flow rate and displacement.

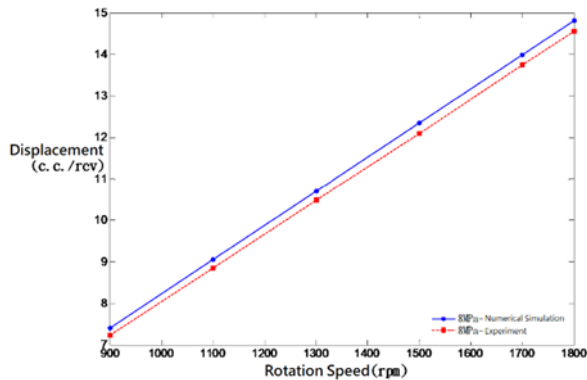


Figure 19 Comparison of simulation and experimental displacement with outlet gauge pressure of 8 MPa

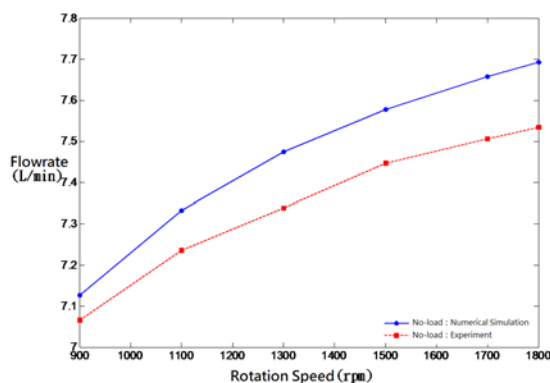


Figure 20 Comparison of simulation and experimental flowrate with outlet gauge pressure at no load

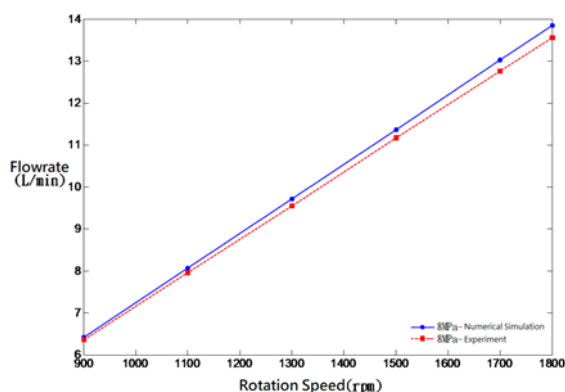


Figure 21 Comparison of simulation and experimental flowrate at outlet pressure of 8MPa

4. Conclusion

In this study, the finite element analysis and experimental verification are investigated to clarify the characteristics of the gear pump flow field. The

important conclusions are as follows:

The outlet flow will decrease as the center distance slightly increases. When the outlet pressure is fixed, the instantaneous outlet mass flow rate changes periodically as the gear rotates. The instantaneous mass flow rate as well as the flow rate amplitude will increase with speed. Higher the rotational speeds can have higher average mass flow rates. This is because the volume of the tooth space is fixed and the flow rate increases with the increase of the rotational speed.

When the rotation speed is fixed with a high outlet pressure, the internal leakage amount increases, and the instantaneous outlet mass flow rate decreases. The higher rotational speed causes the greater irregularity of the outlet mass flow rate.

The simulation and experimental results show that when the outlet gauge pressure is at no-load, its displacement is not affected by the speed, and the flow rate increases as the speed increases. When the outlet gauge pressure is 8 MPa, both the displacement and the flow rate increase with the increase of the speed. On the whole, the outlet flowrate will decrease as the outlet gauge pressure increases.

5. Acknowledgement

This study is partly supported by the Ministry of Science and Technology program number: MOST-106-2221-E-150-018-MY2. The authors thanks the financial support of the project.

6. References

- Castilla, R., Gamez-Montero, P.J. and del Campo, D., "Three-Dimensional Numerical Simulation of an External Gear Pump with Decompression Slot and Meshing Contact Point", *Journal of Fluids Engineering*, Vol. 137, pp.041105-1-041105-10 (2015).
- Castilla, R., Gamez-Montero, P. J., Ertürk, N., Vernet, A., Coussirat, M. and Codina, E., "Numerical Simulation of Turbulent Flow in the Suction Chamber of a Gear pump Using Deforming Mesh and Mesh Replacement", *International Journal of Mechanical Science*, Vol. 52, pp. 1334-1342 (2010).
- Ertürk, N., Vernet, A., Ferré, J. A., Castilla, R., and Codina, E., "Analysis of the Turbulent Flow of an External Gear Pump by Time Resolved Particle Image Velocity", *14th Int Symp on Application of Laser Techniques to Fluid Mechanics*, pp. 1-12 (2008).
- Hooke, C. J. and Koc, E., "End Plate Balance in Gear Pumps", *Proceedings of the Institution of Mechanical Engineers, Part B: Management and engineering manufacture*, Volume: 198, pp. 55-60 (1984).
- Kline, S. and McClintock, F., "Describing Uncertainties in Single-Sample Experiments", *Mechanical*

Engineering, Vol. 75, pp. 3-8 (1953).

Koc, E. and Hooke, C. J., "End Lubrication and Sealing in Gear Pumps with Fixed End Plates", The Journal of Fluid Control, Vol.18-(3), pp. 52-69 (1988).

Koc, E., Kurban, A. O. and Hooke, C. J., "An Analysis of the Lubrication Mechanism of the Bush-Type Bearings in High Pressure Pumps", Tribology International, Vol. 30, No. 8, pp. 553-560 (1997).

Nelik, L., "Operating Conditions and Comparisons between Chemical-Duty Pumps and Specialized High Pressure Gear Pumps", World Pumps, pp. 32-39, (2001 December).

Zakharov, N. N. and Ibragimov, V. I., "Gear Pump with Hydraulically Compensated Face Clearance", Russian Eng. J., Vol.44, No.5, p.26 (1964).

漸開線正齒輪泵之二維流場 數值模擬與實驗驗證

張財壽 王俊捷 張信良

國立虎尾科技大學 動力機械系

摘要

齒輪泵應用範圍相當廣泛，因而以往有許多
的研究進行相關的探討，但鮮少考慮到嚙合點閉合
對於流率之影響。近幾年才開始有研究指出，出口
壓力大時之流場需考慮嚙合點作用，該作用直接影
響數值模擬之出口流率。本研究在此前提下，針對
漸開線正齒輪泵之二維流場特徵進行研究與驗證。
本研究亦搭配齒輪泵測試機台，透過改變轉數、出
口壓力，測量實際輸出容積，並將模擬與實驗結果
相互比較、驗證，實驗結果顯示與理論分析的結果
趨勢是一致的。